Journal of Molecular Liquids 399 (2024) 124444

Contents lists available at ScienceDirect

Journal of Molecular Liquids

journal homepage: www.elsevier.com/locate/molliq

Reduced driving electric field of ionic salt doped nano-structured polymer dispersed liquid crystals device

Srinivas Pagidi [a], Anoop Kumar Srivastava [b], Nidhi Pandey [c], Ramesh Manda [d,*]

[a] Department of Electrical & Electronic Engineering, Southern University of Science and Technology, Xueyuan Road 1088, Nanshan District Shenzhen, Guangdong 518055, China
[b] Department of Applied Science and Humanities, Institute of Engineering & Technology, Dr. Rammanohar Lohia Avadh University, Ayodhya, Uttar Pradesh 224001, India
[c] Department of Physics, United University, Prayagraj, Uttar Pradesh 211012, India
[d] School of Physics, University of Hyderabad, Hyderabad, Telangana 500046, India

ARTICLE INFO

Keywords:
Liquid Crystal
Flexible LCD display
Optically isotropic phase
Phase-separated liquid crystal

ABSTRACT

The nano-structured polymer dispersed liquid crystal (NPDLC) possesses several intriguing properties due to its nano-confined structure and unprecedented flexibility. However, the involved polymer networks necessitate a higher operating field which deteriorates the device's feasibility for real-device applications. Here, we demonstrate a simple technique to reduce the driving field by introducing a small amount of ionic salt into the NPDLC. The selective occupation of ionic salt during the phase separation reduces the interfacial energy of LC molecules, dipping by 40 % (3.6 V/μm) of the driving electric field. The electrohydrodynamic instability created by localized ion transportation led to reduced LC anchoring strength at the polymer interface at which the operating field was reduced. Our design is versatile and a potential alternative to the present NPDLC.

1. Introduction

The nano-structured polymer dispersed liquid crystal (NPDLC) is an emerging and promising technology as it promises unprecedented flexibility and optically isotropic property owing to 3-dimensional geometrical confinement. Furthermore, the optical devices based on NPDLC possess non-trivial fabrication-favored features, such as free from layer alignment, cell gap insensitive, polarization-independent, and fast response time [1,2,3,4]. Taking advantage of the above-mentioned features, various display and photonic devices, such as flexible displays, tunable gratings & lenses, smart windows & shutters, polarization converters, and sensors, have been proposed [1,3,5–9]. Furthermore, a recent demonstration of super-flexible and transparent NPDLC film paves new insights into a rollable display and optical elements [10,11].

The polymerization-induced phase-separation (PIPS) is widely used for fabricating NPDLC as it allows control over the droplet size and morphology, which plays a decisive role in achieving the desired output [2,12–14]. However, it is common practice to employ a high concentration of photo-curable monomers, typically 50 wt% or more, to produce the nano-size LC droplet smaller than a wavelength of visible light, leading to unavoidable stronger surface anchoring interactions of LC with polymer boundary and consequently demanding a higher field to switch between off- & on-states [7,10,15]. Several strategies have been reported by manipulating the boundary interactions to reduce the driving field and reported the lowest driving voltage of 8 V/μm. However, despite several advancements in LC droplet control, due to non-trivial fabrication prerequisite complex structuration, TFT (thin-film-transistor) overdrive technology, and thus, the higher driving field remains unsolved [16–21]. Therefore, in the quest of finding a lower driving voltage of the NPDLC, a facile approach has been made by dispersing ionic salt that selectively occupy the LC and polymer interface during the phase separation and reduces the LC anchoring strength. As a result, the respective driving and threshold fields in ionic salt dispersed NPDLC (IS-NPDLC) are reduced to 3.6 V/μm and 1.4 V/μm, respectively, which is 40 % reduction compared to NPDLC. Furthermore, the transmittance of the system is also significantly improved as the interface localized ionic salts weaken the surface anchoring energy at which the LC molecule can reorient to the field direction for smaller field strengths.

* Corresponding author.
E-mail address: manda_rff@uohyd.ac.in (R. Manda).

https://doi.org/10.1016/j.molliq.2024.124444
Received 22 November 2023; Received in revised form 29 February 2024; Accepted 8 March 2024
Available online 11 March 2024

2. Experimental procedure

2.1. Materials

The NPDLC sample was prepared by mixing 44 wt% of room temperature nematic LC mixture, BL002 ($\Delta\varepsilon$ =17.2 at 1 kHz, $\Delta n = 0.246$ [$n_e = 1.771$, $n_o = 1.5250$], T_{NI} is 74 °C [*Iso* 74 °C *N* −20 °C *Cr*], from Merck), with 27 wt% of pre-polymers TMPTA (Trimethylolpropane triacrylate, refractive index = 1.474, from Sigma-Aldrich) and 27 wt% of EHA (2-Ethylhexyl acrylate, refractive index = 1.436, from Sigma-Aldrich). The nematic LC, BL002, is a eutectic LC mixture of cyanobiphenyls with different alkyl and alkoxy tails and shows LC phase range from 74 °C to −20 °C on cooling. The TMPTA and EHA consist of tri-acrylate and mono-acrylate functionalized pre-polymers. The ionic salt dispersed NPDLC is fabricated by dispersing 2 wt% of tetrabutylammonium tetrafluoroborate (Sigma-Aldrich) into the NPDLC. The photo-initiator Irgacure1173 (1 wt%) was added to samples to initiate photo-polymerization. Since the 42–45 wt% of LC concentration is the best choice for NPDLC [10,22], we have selected 44 wt% of LC in this study.

2.2. Experiments

The experimental procedure for fabrication of IS-NPDLC is schematically shown in Fig. 1. In the first step, the ionic salt is dissolved in a Methanol solution and mixed thoroughly, followed by the addition of LC, monomers, and photo-initiator. After 2 hrs of mixing, the methanol is evaporated under a vacuum, and the final obtained homogeneous mixture is infiltrated into the LC cell by capillary action at 80 °C. Then, the phase-separation process is initiated by irradiating 100 mW/cm^2 of ultra-violet light for 20 min at 80 °C. We employed an in-plane switching (IPS) cell that consists of a patterned indium-tin-oxide bottom substrate with specific electrode width (w) (4 μm) and spacing (l) (4 μm), while no electrodes on the top substrates. Both substrates are uniformly separated by 8 μm film spacer. After the phase-separation process, several characterizations were performed, and finally, the two substrates were separated to peel off the IS-NPDLC film for further investigation.

The scattering level of the samples is estimated by measuring wavelength-dependent transmission using a UV–Visible spectrometer (Jasco, V-760). The optically isotropic phase was identified and textures were captured for further characterization by using a polarization optical microscope (POM) (Nikon, Eclipse LV100POL) with crossed polarizers and an attached digital camera. The square-wave signal with appropriate frequency is generated and supplied to the sample by using Function Generation (Tektronix, AFG3101C) and Signal Amplifier (FLC Electronics, A400). The field-dependent transmittance of the samples was measured by a lab-made He-Ne laser (wavelength is 632 nm) with crossed Glan-Thompson polarisers set up at which the emitted light is detected by a photodiode and a digital oscilloscope (Tektronix, DPO2024B). The dielectric measurements were performed using an impedance analyzer (Novocontrol, Alpha-A). In the final step, the microstructural characterization was performed by using a field emission scanning electron microscope (FESEM) (ZEISS, Ultra-55).

3. Results and Discussion

In the first step, the scattering level of the samples is estimated by measuring wavelength-dependent transmission and compared with the pre-polymerization state. As illustrated in Fig. 2, the pre-polymerization sample shows ~ 90 % of transmittance. The remaining 10 % transmittance is affected by the substrates and the patterned electrodes on them. The pristine NPDLC sample exhibits a maximum of ~ 80 % transmittance at longer wavelengths. It indicates optimization of droplet size along with refractive index match was achieved. From Rayleigh-Gans scattering theory, which describes the scattering of NPDLC, such as high transparency originates from the smaller droplet size and the refractive index match between the LC droplet (n_{avg}) and the polymer matrix (n_p). Our NPDLC system shows 50 % transmittance for visible range wavelengths and even less in UV wavelengths. The transmittance of the samples tends to decrease with decreasing wavelength. This tendency could originate from increased light scattering for shorter wavelengths as the incident light reaches close to the dimensions of the droplet size. We presume that the level of cross-linking of monomers is higher as these monomer combinations are designed for a high polymerization rate. The system exhibits optically isotropic in the absence of a field. Thus, it exhibits isotropic refractive index (n_i), which is the ratio of n_{avg} and n_p and corresponding volume fractions of LC and monomers. However, the incident polarization encounters an effective refractive index (n_θ) $\left(n_\theta = n_e n_o / \sqrt{n_e^2 cos^2\theta + n_o^2 sin^2\theta}\right)$, where θ is the angle of incident polarization. The magnitude of n_θ varies between n_o and n_e,

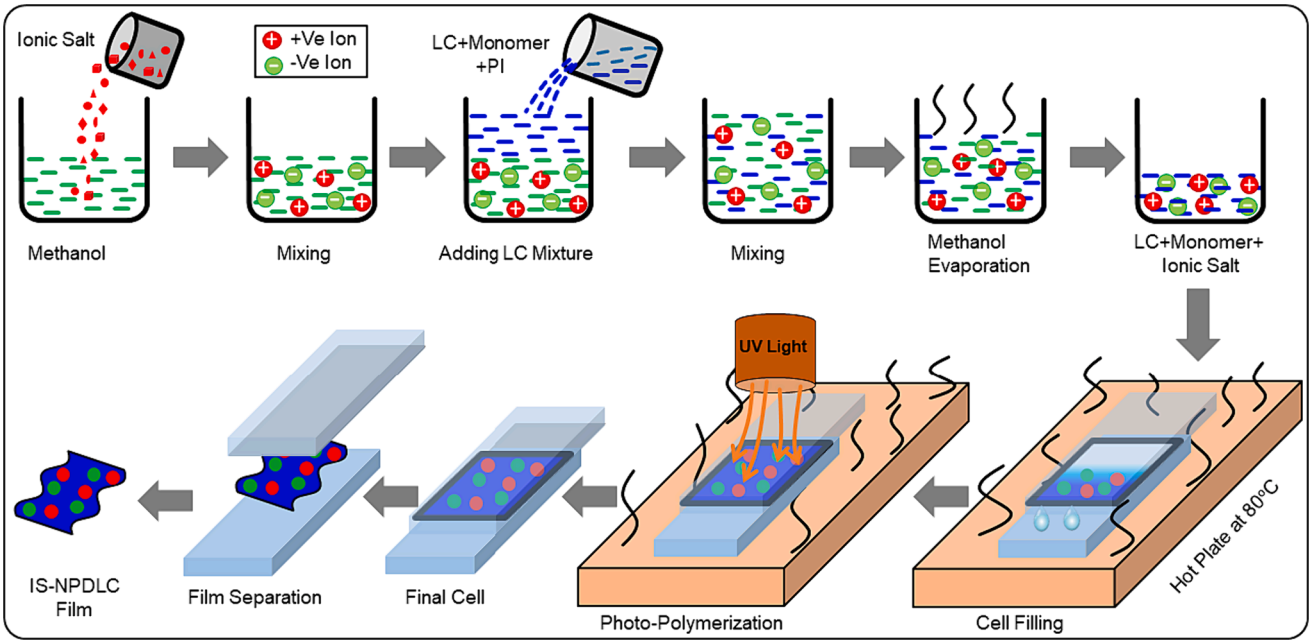

Fig. 1. The schematic of the experimental procedure for fabricating IS-NPDLC.

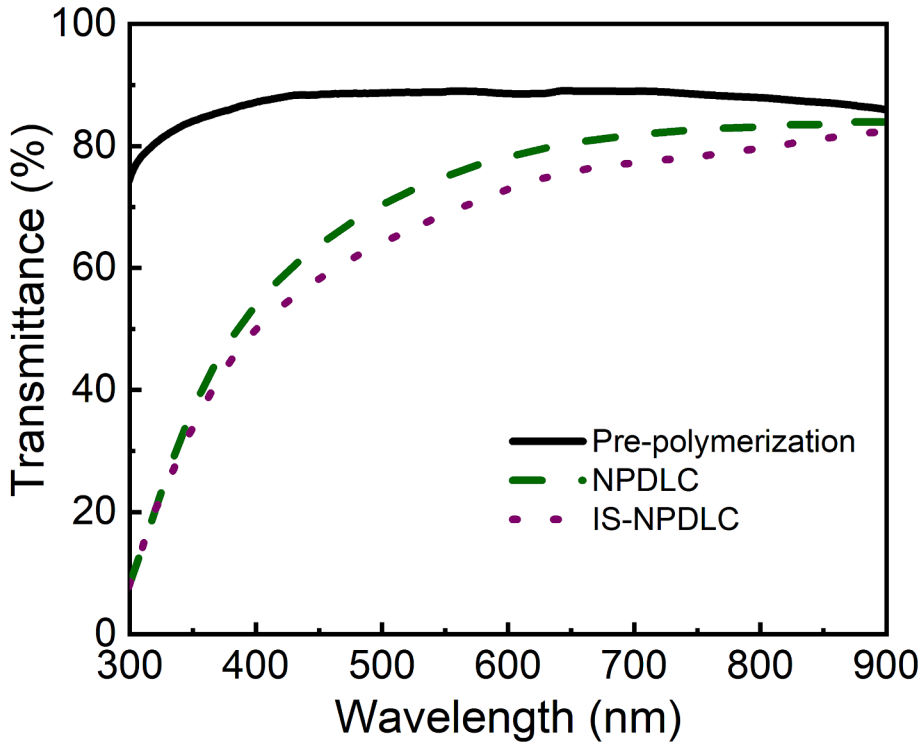

Fig. 2. Wavelength-dependent transmittance spectra of NPDLC (dashed line) and IS-NPDLC (dotted line). The solid black line indicates the transmittance before the phase separation of LC.

while the n_i varies from n_p to n_{avg}. Here, the n_{avg} and n_p are 1.607 and 1.455, respectively. Since the n_{avg} and n_p difference is negligible, wavelength-dependent transmittance reduction for NPDLC is presumed to originate from increased material absorption due to polymerization and residual photo-initiator. Remarkably, adding ionic salt to NPDLC causes a < 10 % transmittance decrease in the green and red wavelength

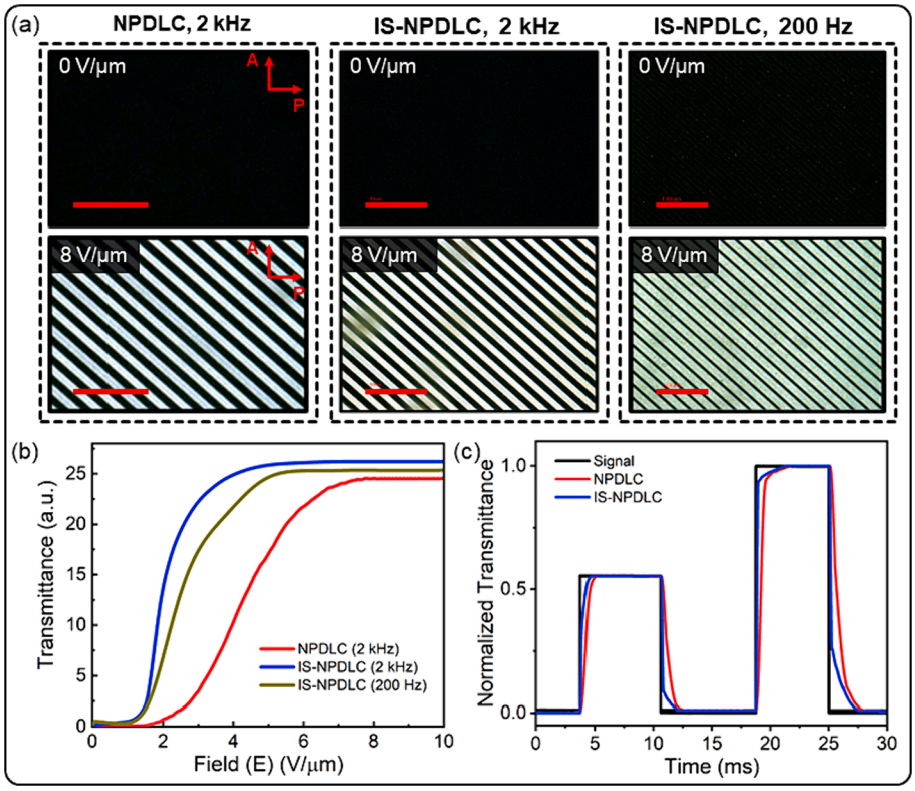

Fig. 3. (a) Switching of NPDLC and IS-NPDLC at 2 kHz and IS-NPDLC at 200 Hz. The scale bar in POM images is 50 μm. P: polarizer; A: analyzer. (b) Field-dependent transmittance of NPDLC and IS-NPDLC at 2 kHz and 200 Hz. (c) The time-dependent reorientation and relaxation mechanism of both samples.

bands while unaffected in UV and infrared regions. Such transmission reduction in IS-NPDLC is thought to have originated from the droplet size alteration that occurred during phase separation due to ionic strength and miscibility, not due to a mismatch between n_{avg} and n_p.

Next, phase identification and electro-optical measurement are performed by observing the optical textures under crossed polarisers using a POM. The optical textures of both NPDLC and IS-NPDLC appear black under crossed polarizers and remain black on sample rotation, suggesting the obtained phase is optically isotropic (Fig. 3a). There is no indication of significant light leakage. Next, the required 2 kHz square wave field is supplied by a function generator and amplifier while observing the optical textures with POM. The applied field (E) corresponds to V/l, where V and l are the applied voltage and the electrode gap, respectively. We considered field strength instead of voltage to avoid the cell gap sensitivity on the threshold field (E_{th}) and operating field (E_{op}). The optical textures turned brighter once a sufficient field was provided. The brightness due to induced birefringence along the field direction is spatially uniform between the IPS electrodes. This unusual phenomenon can be explained by the adopted Kerr effect described by $\Delta n_{ind}(E) = K\lambda E^2$, where K is the Kerr constant, λ is the wavelength of the incident light, and E is the applied field. The detailed switching mechanism of NPDLC in IPS mode can be found elsewhere [10,11]. The signal frequency was reduced to 200 Hz to observe the frequency dependency of Δn_{ind}. The brightness between the electrode strips indicates the reorientation of the LC molecules towards the field direction, which is slightly higher for IS-NPDLC. This remarkable phenomenon can be understood from the frequency-dependent response of the IS-NPDLC. The increased width of the bright strips indicates more LC molecules are responding to the applied field. To see more insight, the field-dependent transmittance was then measured by irradiating a He-Ne laser beam on the sample under crossed Glan-Thomson polarizers and subsequently detecting the transmitted intensity by a photo-diode and digital oscilloscope. The electro-optical measurements reveal that manifestation of Δn_{ind} appears after a threshold field and saturates for higher fields (Fig. 3b). The E_{th} and E_{op} are defined as fields corresponding to 10 % and 90 % of peak transmittance, respectively. The E_{op} of NPDLC and IS-NPDLC for 2 kHz are 6.7 V/μm and 3.6 V/μm, respectively. Interestingly, the E_{op} of IS-NPDLC is relatively increased to 4.7 V/μm by decreasing the applied frequency to 200 Hz. The E_{th} of NPDLC and IS-NPDLC are 2.3 V/μm and 1.4 V/μm for 2 kHz, respectively. And, the E_{th} is unchanged for reducing frequency to 200 Hz. For the IS-NPDLC sample, we achieved a 40 % reduction of both E_{op} and E_{th}. The obtained data suggest that the reduction in E_{op} is associated with ionic salts. Remarkably, the peak transmittance of IS-NPDLC significantly increases for 2 kHz, which tends to be reduced for 200 Hz. This reveals that if the frequency increases, the transmittance also increases. This unusual behavior is thought to be originated from the weak surface anchoring and strong dipolar reorientation of LC molecules generated for ionic salts under high frequency; thus, the number of reoriented LC is increased with frequency.

The dispersed ionic salt also significantly affects both the reorientation and relaxation mechanisms. Both samples are supplied with a 2 kHz random pulsed signal with different amplitudes and measured time-dependent response as shown in Fig. 3c. The rise response time (τ_r) that corresponds to the time required for 10 % to 90 % transmittance on field supply is estimated as 2.3 ms and 1.8 ms for NPDLC and IS-NPDLC, respectively. The decay response time (τ_d), the time taken for 90 % to 10 % transmittance change upon field removal, is measured as 2.4 ms and 1.8 ms for NPDLC and IS-NPDLC, respectively. The relative change in the τ_r and τ_d reveals the possible reduction of surface anchoring due to in-plane ion oscillations in response to the IPS field.

Further, we measured the ionic conductivity of NPDLC and IS-NPDLC from dielectric spectroscopy in order to investigate the effect of ions in IS-NPDLC as compared to NPDLC. Dielectric permittivity (ε') and dielectric loss (ε'') were measured in the frequency (f) range of 1.0 Hz to 10.0 MHz. Though, no dielectric relaxations were observed in the dielectric spectra, however, both ε' and ε'' were increased with decreasing frequency in low-frequency region (1–100 Hz) in which the former is due to electrode polarization capacitance and latter is due to ionic conductivity [23,24]. Fig. 4 shows the variation of ε'' with frequency in the low-frequency region (1–100 Hz) for NPDLC and IS-NPDLC. The ε'' as a function of frequency can be expressed as: $\varepsilon'' = \frac{G}{2\pi\varepsilon_o f C_o}$, where G is a conductance, C_o is an air capacitance and ε_o (=8.85 pF/m) is the free space permittivity [23,24]. As conductivity (σ) can be expressed as $\sigma = G/C_o$, therefore:

$$\varepsilon'' = \frac{\sigma}{2\pi\varepsilon_o f} \tag{1}$$

The σ was estimated by fitting into the experimental data with Eq. (1), as shown in Fig. 4a-b. The estimated σ of NPDLC and IS-NPDLC were 2.5×10^{-7} S/m and 3.4×10^{-7} S/m, respectively. This value reveals that the number of ions in the IS-NPDLC system is slightly higher than in the NPDLC. Small increased σ means resistivity is reduced and it will ease the LC molecules to orient under electric field. This could be another possible reason for getting reduced E_{op} in IS-NPDLC compared to NPDLC. In order to probe the reason of higher transmittance for IS-NPDLC as compared to NPDLC, the variation of ε'' with frequency is plotted in Fig. 4c. In the Inset (100 Hz to 3 kHz), it could be easily seen that though the loss in IS-NPDLC is higher as compared to NPDLC, nevertheless the ε'' in case of NPDLC increases with decrease in frequency whereas in case of IS-NPDLC, the ε'' is fairly stable with frequency. Hence, the ions are quite screened in IS-NPDLC, which in turn increases the transmission. The slight increase in the transmission at 2 kHz as compared to 200 Hz for IS-NPDLC, might be due to the slight change in corresponding dielectric data. The ε'' at 200 Hz and 2 kHz were 127.2 and 126.8, respectively. The ε' at 200 Hz and 2 kHz were 61.8 and 61.6 respectively.

After finishing all necessary characterizations, the substrates are detached, and the sample is peeled-off. The peel-off can easily be achieved by a few heating cycles above 80 °C. From Fig. 5a-b, our NPDLC film is brittle as it breaks into pieces during the peel-off, while the IS-NPDLC shows similar stability. In principle, the NPDLC phase possesses unprecedented flexibility due to stronger LC confinement by the polymer network. But here, the NPDLC film achieves brittleness and breaks into smaller pieces. A similar trend was noticed for IS-NPDLC. The brittleness could be originated from the strong interaction with the substrate and possible contamination due to the solution used for ionic salt dispersion. The film fabrication process can be improved by surface coating of substrates [11]. Finally, the LC was extracted from the film by keeping the cell in hexane for two days, followed by morphological studies using the FESEM. From the morphology images shown in Fig. 5c-d, it is clear that the dense polymer matrix with a void size smaller than 400 nm is formed for both cases. This data reveals that the dispersed ionic salts do not affect the polymer matrix formation. The micrograph indicates a relatively low LC fill factor of ~ 35 % due to low LC concentration. However, the sample shows enough electro-optic effect sufficient for device applications.

The schematic representation of the driving mechanism of NPDLC and IS-NPDLC is presented in Fig. 5e. In principle, the field response of LC in NPDLC is associated with the interplay between surface anchoring interactions, elastic forces, and dielectric strengths. Among these, the surface anchoring force is dominated due to nano-scale geometric confinement. The free energy of the NPDLC system can be described by the elastic (f_{elas}), electric (f_{ele}), and surface (f_{surf}) free energy densities [25]. The f_{ele} is nonlinear with applied field E and governed by the dielectric interactions. The $f_{surf}\left(=-\frac{1}{2}W_s\sin^2\alpha\right)$, where W_s is the surface anchoring strength of LC and α is the orientation angle of LC, depends on the LC orientation and anchoring strength at the polymer surface. The f_{surf} cannot be neglected for tiny droplets like NPDLC and IS-NPDLC. The

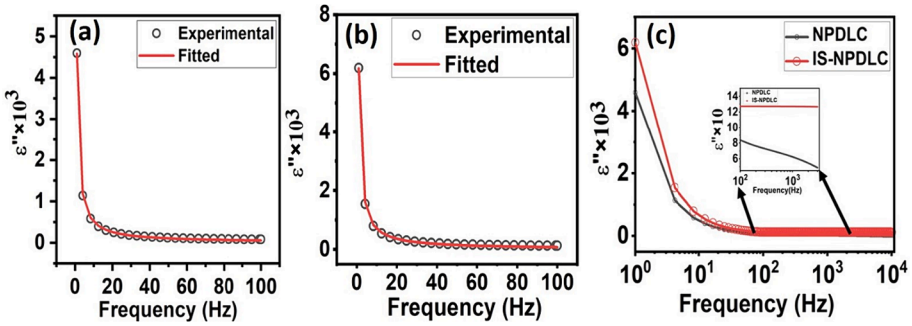

Fig. 4. Variation of dielectric loss ($\varepsilon^{''}$) as a function of frequency in low-frequency region of 1 to 100 Hz; (a) NPDLC, and (b) IS-NPDLC. Circles show the experimental data whereas the continuous red line indicates the best fit of Eq. (1). (c). Variation of $\varepsilon^{'}$ as a function of frequency in the frequency region of 1 Hz to 10 kHz.

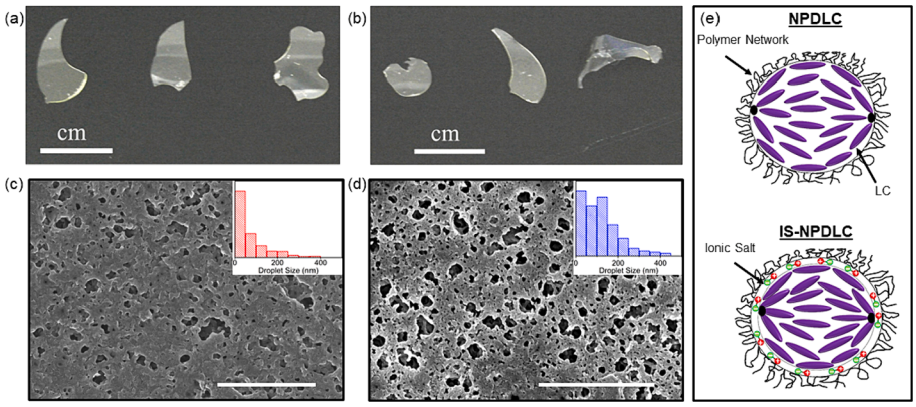

Fig. 5. The obtained film of NPDLC (a) and IS-NPDLC (b). Morphology of (c) NPDLC and (d) IS-NPDLC. The droplet size distribution is shown inset of each micrograph. The scale bar is 2 μm. (e) Schematic representation of the driving mechanism of NPDLC and IS-NPDLC.

dielectric torque should overcome both the f_{elas} and f_{surf} to align the LC molecules along the field direction. By considering the droplet is spherical, the required threshold electric field strength to reorient the LC molecules is denoted as:

$$E_{th} = \sqrt{\frac{1}{\varepsilon_o \Delta\varepsilon R}\left(\frac{W_s}{2\pi} - \frac{k_{eff}}{\pi R}\right)} \tag{2}$$

where R and k_{eff} are the average size of the LC droplet and the effective elastic constants of LC. Further, we calculated the W_s from Eq. (2) by considering k_{eff} is 10 pN. The obtained W_s of NPDLC and IS-NPDLC are 125×10^{-4} Nm^{-1} and 44×10^{-4} Nm^{-1}, respectively. These results reveal a significant decrease of W_s is obtained for IS-NPDLC. When ionic salts are added to the NPDLC, it is obvious that the salt traps between LC and polymer network interface. There is a high possibility of ions trapping between the LC and polymer network rather than deep inside the droplet. The ions in NPDLC are confined by polymer walls and abide to move within the droplet [26,27]. Our discussion is constrained to the spherical bipolar droplets that consist of point defects on the opposite sides of the surface. The surface defects of bipolar droplets are highly energetic singular points; thus, there is a high possibility of ionic salts occupying these point defects' vicinity. In addition, there is a high possibility of forming nanochannels for ion transportation since the doped ionic salt is free to move, creating turbulence and subsequent electrohydrodynamic instability. We presume that this electro-hydrodynamic instability is localized at the LC and polymer interface, which reduces LC anchoring strength W_s. For IS-NPDLC, there is a high possibility of guided movements of salts under field strengths that decrease the LC anchoring strength W_s, leading to a 40 % decrease of both E_{op} and E_{th}, which could be a competitive record compared to similar literature reported elsewhere [10,11,14,21,28]. Our conductivity measurements reveal that there is a significant improvement in ionic conductivity. The reduced E_{op} and E_{th} originated from the resultant effect of both ionic conductivity and reduced anchoring. The reduced E_{th} (1.4 V/μm) and E_{op} (3.6 V/μm) of the proposed system allows TFT to drive without need of any overdrive technology.

4. Conclusion

A facile technique to reduce the driving field of NPDLC is demonstrated by dispersing a small number of ionic salts. The dispersed ionic salts selectively trap between the LC and polymer interface and reduce the LC anchoring strength. As a result, we reduced the operating field to 3.6 V/μm (40 %) for 2 wt% of suitable ionic salt. Furthermore, our design also reduces the threshold voltage and increases the peak transmittance by increasing frequency. Therefore, this technique could be a potential alternative for improving electro-optical parameters such as operating/driving voltage and transmittance of NPDLC.

Funding

This work is supported by the Ramanujan Fellowship (RJF/2022/000094), Science and Engineering Research Board (SERB), India.

CRediT authorship contribution statement

Srinivas Pagidi: Formal analysis, Data curation. **Anoop Kumar Srivastava:** Writing – original draft. **Nidhi Pandey:** Formal analysis. **Ramesh Manda:** Supervision, Funding acquisition, Conceptualization.

Declaration of competing interest

The authors declare that they have no known competing financial interests or personal relationships that could have appeared to influence the work reported in this paper.

Data availability

Data will be made available on request.

Acknowledgment

We thank Prof. Surajit Dhara (University of Hyderabad) for his valuable discussion and comments.

References

[1] P.S. Drzaic, Reorientation dynamics of polymer dispersed nematic liquid crystal films, Liq. Cryst. 3 (11) (1988) 1543–1559.
[2] Drzaic P.S., Liquid crystal dispersions. 1995.
[3] S. Pagidi, R. Manda, S.S. Bhattacharyya, S.G. Lee, S.M. Song, Y.J. Lim, J.H. Lee, S. H. Lee, Fast switchable micro-lenticular lens arrays using highly transparent nano-polymer dispersed liquid crystals, Adv. Mater. Interfaces 6 (18) (2019) 1900841.
[4] M.H. Saeed, S. Zhang, Y. Cao, L. Zhou, J. Hu, I. Muhammad, J. Xiao, L. Zhang, H. Yang, Recent advances in the polymer dispersed liquid crystal composite and its applications, Molecules 25 (23) (2020) 5510.
[5] Doane, J. W. In Liquid Crystals: Applications and Uses; Bahadur, B., Ed.; World Scientific: Singapore, 1990; Vol. 1.
[6] A.J. Lovinger, K.R. Amundson, D.D. Davis, Morphological investigation of UV-curable polymer-dispersed liquid-crystal (PDLC) materials, Chem. Mater. 6 (10) (1994) 1726–1736.
[7] R. Manda, S. Pagidi, S.S. Bhattacharyya, C.H. Park, Y.J. Lim, J.S. Gwag, S.H. Lee, Fast response and transparent optically isotropic liquid crystal diffraction grating, Opt. Express 25 (20) (2017) 24033–24043.
[8] S. Kumar, H. Hong, W. Choi, I. Akhtar, M.A. Rehman, Y. Seo, Acrylate-assisted fractal nanostructured polymer dispersed liquid crystal droplet based vibrant colored smart-windows, RSC Adv. 9 (22) (2019) 12645–12655.
[9] L.V. Natarajan, C.K. Shepherd, D.M. Brandelik, R.L. Sutherland, S. Chandra, V. P. Tondiglia, D. Tomlin, T.J. Bunning, Switchable holographic polymer-dispersed liquid crystal reflection gratings based on thiol-ene photopolymerization, Chem. Mater. 15 (12) (2003) 2477–2484.
[10] R. Manda, S. Pagidi, Y.J. Lim, R. He, S.M. Song, J.H. Lee, G.D. Lee, S.H. Lee, Self-supported liquid crystal film for flexible display and photonic applications, J. Mol. Liq. 291 (2019) 111314.
[11] R. Manda, J.H. Yoon, S. Pagidi, S.S. Bhattacharyya, D.T. Tran, Y.J. Lim, J. M. Myoung, S.H. Lee, Paper-like flexible optically isotropic liquid crystal film for tunable diffractive devices, Opt. Express 27 (24) (2019) 34876–34887.
[12] G.W. Smith, Cure parameters and phase behavior of an ultraviolet-cured polymer-dispersed liquid crystal, Mol. Cryst. Liq. Cryst. 196 (1) (1991) 89–102.
[13] R.R. Deshmukh, M.K. Malik, Effect of temperature on the optical and electro-optical properties of poly (methyl methacrylate)/E7 polymer-dispersed liquid crystal composites, J. Appl. Polym. Sci. 109 (1) (2008) 627–637.
[14] K. Li, H. Jiang, M. Cheng, Y. Li, Z. Yin, D. Luo, X.W. Sun, Y.J. Liu, Controlling morphological and electro-optical properties via the phase separation in polymer/liquid-crystal composite materials, Liq. Cryst. 47 (2) (2020) 238–247.
[15] S. Aya, K.V. Le, F. Araoka, K. Ishikawa, H. Takezoe, Nanosize-induced optically isotropic nematic phase, Jpn. J. Appl. Phys. 50 (5R) (2011) 051703.
[16] Z. Shi, Z. He, C. Li, Z. Miao, D. Wang, Y. Luan, Y. Li, Y. Zhao, The role of nanomesh fibres loaded with fluorescent materials on the electro-optical performance of PDLC devices, Liq. Cryst. 49 (15) (2022) 2037–2050.
[17] S. Pagidi, R. Manda, S.S. Bhattacharyya, K.J. Cho, T.H. Kim, Y.J. Lim, S.H. Lee, Superior electro-optics of nano-phase encapsulated liquid crystals utilizing functionalized carbon nanotubes, Compos. B Eng. 164 (2019) 675–682.
[18] N. Nasir, H. Hong, M.A. Rehman, S. Kumar, Y. Seo, Polymer-dispersed liquid-crystal-based switchable glazing fabricated via vacuum glass coupling, RSC Adv. 10 (53) (2020) 32225–32231.
[19] C.C. Hsu, Y.X. Chen, H.W. Li, J.S. Hsu, Low switching voltage ZnO quantum dots doped polymer-dispersed liquid crystal film, Opt. Express 24 (7) (2016) 7063–7068.
[20] B. Kim, H.G. Kim, G.Y. Shim, J.S. Park, K.I. Joo, D.J. Lee, J.H. Lee, J.H. Baek, B. K. Kim, Y. Choi, H.R. Kim, Fast-switching optically isotropic liquid crystal nano-droplets with improved depolarization and kerr effect by doping high k nanoparticles, Appl. Opt. 57 (2) (2018) 119–129.
[21] S.J. Shivaraja, M. Sahai, R.K. Gupta, V. Manjuladevi, Superior electro-optical switching properties in polymer dispersed liquid crystals prepared with functionalized carbon nanotube nanocomposites of LC for switchable window applications, Opt. Mater. 137 (2023) 113546.
[22] R. Manda, S. Pagidi, M. Kim, C.H. Park, H.S. Yoo, K. Sandeep, Y.J. Lim, S.H. Lee, Effect of monomer concentration and functionality on electro-optical properties of polymer-stabilised optically isotropic liquid crystals, Liq. Cryst. 45 (5) (2018) 736–745.
[23] A.K. Srivastava, V.K. Agrawal, R. Dabrowski, J.M. Otón, R. Dhar, Electro-optical and dielectric relaxation studies of an antiferroelectric liquid-crystal mixture (W-132A), J. Appl. Phys. 98 (1) (2005) 013543.
[24] A.K. Srivastava, R. Dhar, V.K. Agrawal, S.H. Lee, R. Dabrowski, Switching and electrical properties of ferro-and antiferroelectric phases of MOPB (H) PBC 2008, Liq. Cryst. 35 (9) (2008) 1101–1108.
[25] Vicari L. Optical applications of liquid crystals. 2016, CRC Press.
[26] K.W. Lin, H.Y. Tseng, L.M. Chang, C.C. Li, C.T. Wang, T.H. Lin, Mechanism of scattering bistable light valves based on salt-doped cholesteric liquid crystals, Opt. Express 29 (25) (2021) 41213–41221.
[27] L.M. Chang, K.W. Lin, H.Y. Tseng, C.C. Li, D.Y. Guo, H.C. Jau, C.T. Wang, T.H. Lin, Multifunctional liquid crystal Smart glass with light field shaping, dimming, and scattering control, Advanced Photonics Research. 3 (8) (2022) 2100344.
[28] S.G. Kang, J.H. Kim, Optically-isotropic nanoencapsulated liquid crystal displays based on kerr effect, Opt. Express 21 (13) (2013) 15719–15727.